

A Novel Route to Defect Turbulence in Nematics

P. E. Cladis,¹ Cécile Fradin,^{1,2} P. L. Finn¹ and Helmut R. Brand^{1,3}

1. Advanced Liquid Crystal Technologies, POB 1314, Summit, NJ 07902 USA
2. Physique de l'État Condensé, CEA Saclay, F91191 Gif-sur-Yvette Cedex, France
3. Theoretische Physik III, Universität Bayreuth, D-95440 Bayreuth, Germany

A novel cascade of instabilities involving 3 wavelength doubling transitions to turbulent patterns has been observed in EHC when the director boundary conditions are homeotropic and there is no flow alignment. Above the Fréedericksz transition, the first instability is an oscillatory pattern with the roll axes at an angle to the director. At slightly higher voltages there is a transition to a Standing Stripe Pattern that in turn transforms to a curved roll pattern nucleated by a regular array of $S=+1/2$ line defects (Möbions). We call this pattern the Zvinger pattern, a cage for wild animals, the $S=+1/2$'s. These observations provide important complementary information for theories based on small amplitude perturbations of a highly nonlinear base state.

Keywords: Pattern Formation, Nematics, Flow Alignment

INTRODUCTION

The discussion presented here is a slightly more detailed version of the subharmonic (wavelength doubling) cascade which has recently been published [1]. This wavelength doubling sequence is a new route to spatio-temporal disorder. It was observed in a nematic liquid crystal with a negative dielectric anisotropy and prepared with homeotropic boundary conditions. With these boundary conditions, the electrohydrodynamic convection patterns (EHC) are built on a high nonlinear base state for which the director, \mathbf{n} , has complete rotational freedom in planes perpendicular to the driving force, an AC electric field, \mathbf{E} . These observations are in striking contrast to typical EHC patterns built on the initially uniform base state provided by homogeneous boundary conditions [2]. Among the remarkable features of this cascade are the Standing Stripe Pattern and the Zvinger Pattern nucleated by disclinations of only one topological charge, $S = +1/2$ (Möbions). In the Standing

Stripe Pattern, \mathbf{n} has a small amplitude modulation parallel to the roll axes, \mathbf{R} . In the Zvinger Pattern, named to suggest a cage for wild animals, \mathbf{n} rotates 2π in a Zvinger wavelength, λ_Z . As disclinations of only one topological charge are present, when the external driving force is removed from the Zvingers, a state with a length scale emerges that coarsens by defect motion extremely slowly to the uniform state (Fig. 2).

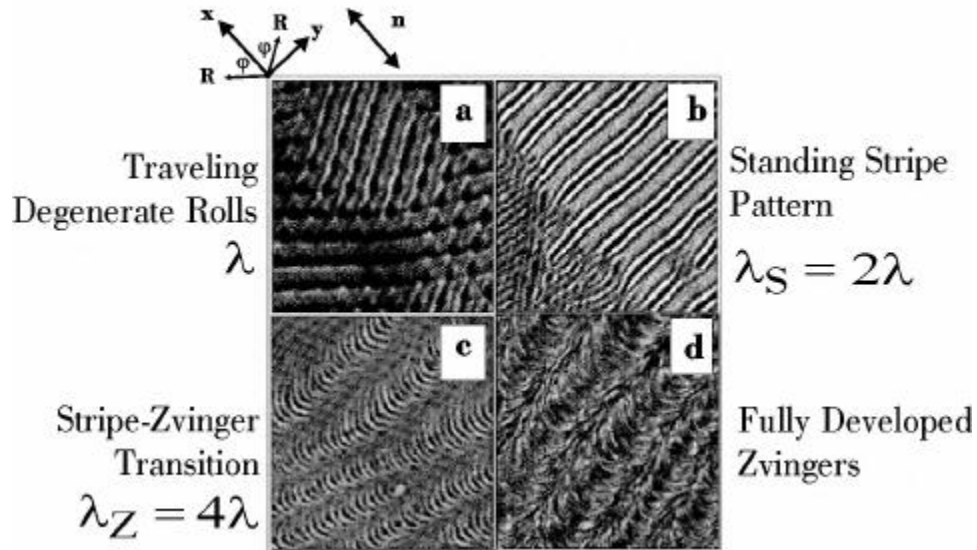


Fig. 1. The wavelength doubling cascade [1]. Control parameters are the applied voltage, V , and frequency, ν .

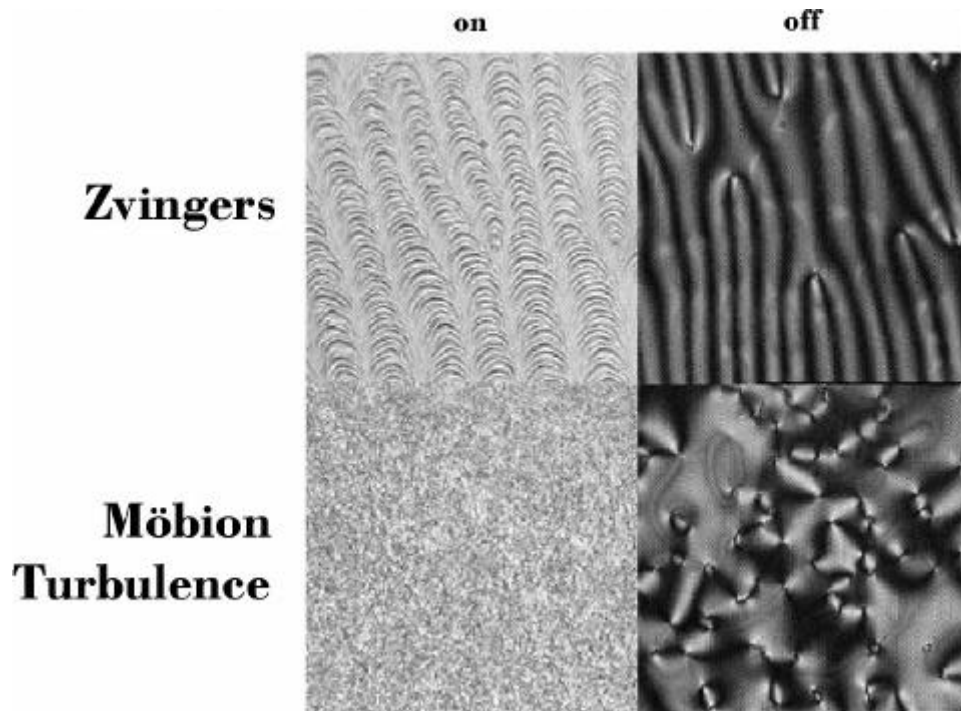


Fig. 2. Zvinger and Möbion Turbulence patterns when the voltage is on (left) and off (right) [1].

Wavelength Doubling to Möbius Defect Turbulence

In the Möbion turbulence pattern (Fig. 2), defects are larger in number and irregularly distributed. The fastest way to recover the initial homeotropic orientation from Möbion turbulence is to heat to the isotropic liquid then cool back to the nematic phase.

EXPERIMENTAL DETAILS

The instability studied is EHC where an AC electric field, \mathbf{E} , is applied to a thin nematic layer (thickness $d = 10\text{--}20\ \mu\text{m}$) [3,4] with a negative dielectric anisotropy, $\epsilon_a < 0$: in a large enough field, $\mathbf{n} \perp \mathbf{E}$. The frequency, ν , of the applied field is such that $\nu < \nu_c$ so that charge motion creating the convective flow field follows \mathbf{E} . $\nu_c \approx 450\ \text{Hz}$ is experimentally determined [5]. As usual, the instabilities are viewed along \mathbf{E} through transparent electrodes using a polarizing microscope interfaced to a video camera and computer controlled image analysis system. The material studied is 10E6 [2,5,6,7] at a temperature where the rotational viscous coefficient, $\gamma_1 < |\gamma_2|$, the extensional viscous coefficient, so that there is no flow alignment [2, 3]. This wavelength doubling cascade has not been predicted by theory [8] nor observed in materials where $\gamma_1 > |\gamma_2|$ [9,10].

UNIFORM BASE STATE: HOMOGENEOUS BOUNDARY CONDITIONS

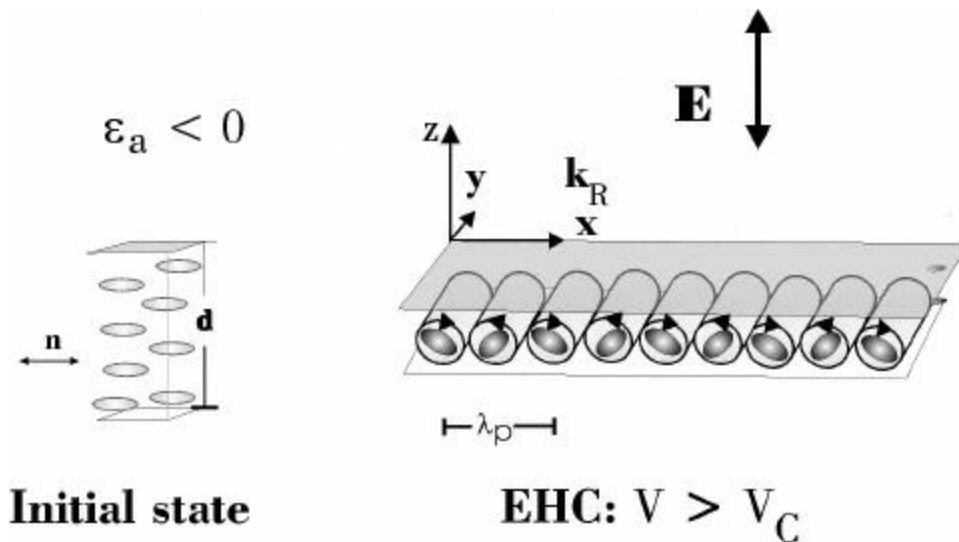


Fig. 3. In traditional EHC where \mathbf{n} is initially uniform and parallel to the transparent electrodes, the pattern is a small amplitude perturbation of a uniform state.

Nor has this wavelength doubling cascade (Fig. 1) been observed in samples where boundary conditions define a preferred direction, \mathbf{x} , with $\mathbf{n} \parallel \mathbf{x}$ (Fig. 3) [2]. For these boundary conditions, the pattern is a small amplitude perturbation of a uniform state. The observation [2] is that the onset of EHC when the applied voltage $V \gtrsim V_C$ is consistent with a predicted [4] forward bifurcation to stationary normal rolls, i.e. the roll axis, $\mathbf{R} \perp \mathbf{k}_R$, the roll wavevector shown in Fig. 3, is normal to \mathbf{n} : $\mathbf{R} \perp \mathbf{n}$. When

the frequency of the applied voltage, $\nu \cong 10\text{Hz.}$, the pattern wavelength, $\lambda_p \approx d$. λ_p decreases to $\lambda_p \approx d/2$ when $\nu \cong 350\text{Hz}$ [2]. In this same range of frequencies, $12\text{V} < V_C < 40\text{V}$.

NONLINEAR BASE STATE – HOMEOTROPIC BOUNDARY CONDITIONS

In the case of homeotropic boundary conditions (Fig. 4), \mathbf{n} is initially parallel to \mathbf{E} . As torques exerted on \mathbf{n} by \mathbf{E} compete with those from boundary conditions, there is a boundary layer of thickness, $\xi \propto 1/E \sim 0.5\text{-}2 \mu\text{m}$ in these experiments. This fluid boundary layer allows \mathbf{n} complete rotational freedom in planes $\perp \mathbf{E}$.

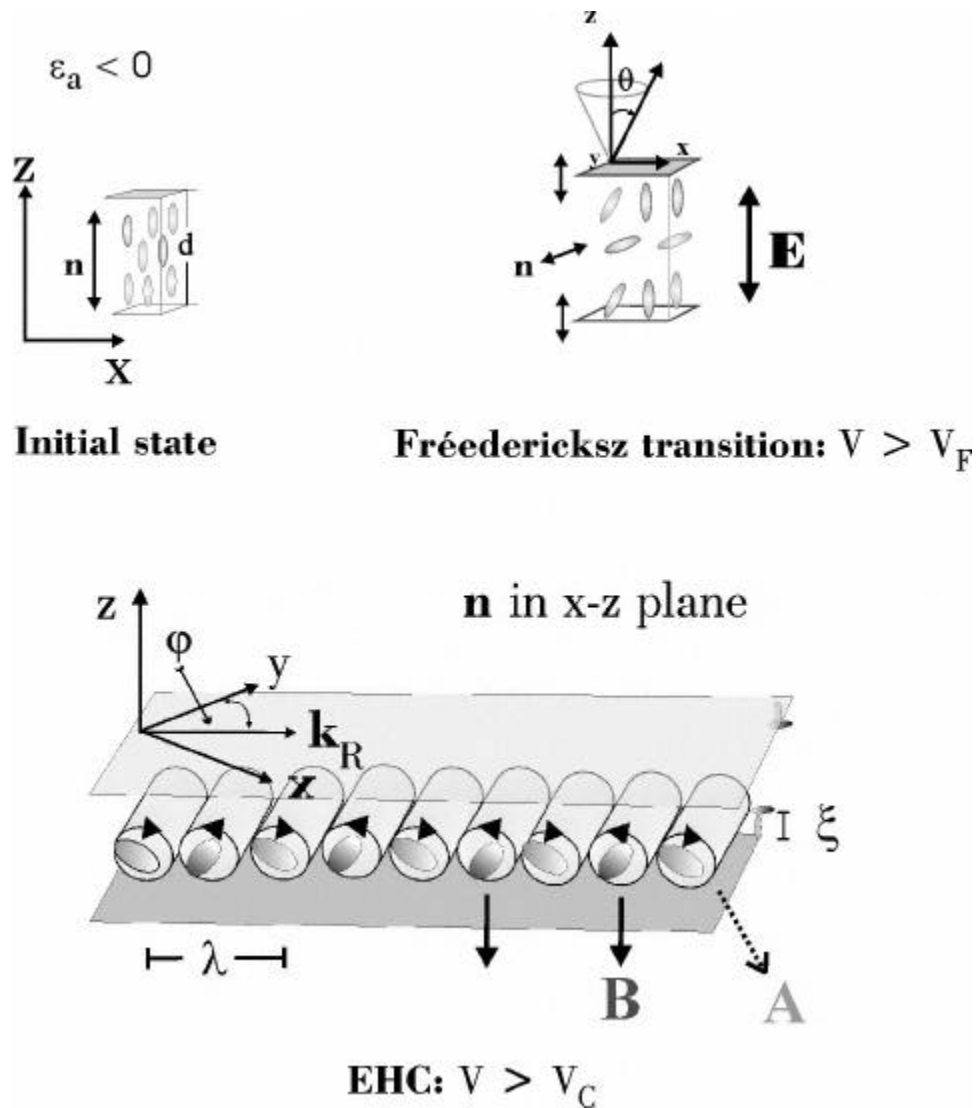


Fig. 4. With homeotropic boundary conditions, the curvature elasticity for \mathbf{n} is highly nonlinear well before electroconvection onset [1].

Wavelength Doubling to Möbius Defect Turbulence

When the applied voltage $V > V_F$, the Fréedericksz transition voltage, \mathbf{n} acquires a component, n_x , in the sample mid-plane $\perp \mathbf{E}$: $\theta > 0$ (Fig. 4). While n_x can be anywhere in the xy -plane, to minimize its elastic energy with well-prepared homeotropic boundary conditions, an x -direction is locally quickly selected so that variations in \mathbf{n} are only in an xz -plane (Fig. 4). With increasing V , $\theta \rightarrow \pi/2$. As $\theta > \pi/2$ launches known director instabilities [3], not observed in these experiments, we take $\theta = \pi/2$ as an upper bound. As is well-known, the Fréedericksz transition sets up a highly nonlinear state for the curvature elasticity of \mathbf{n} well before convection onset at $V_C \gtrsim 2 V_F$.

In the roll pattern shown in Fig. 4, we distinguish two kinds of rolls. We call rolls in which viscous and dielectric torques work together, A rolls, and those in which they compete, B rolls (Fig. 5). We use this idea to estimate the speed at which the pattern travels.

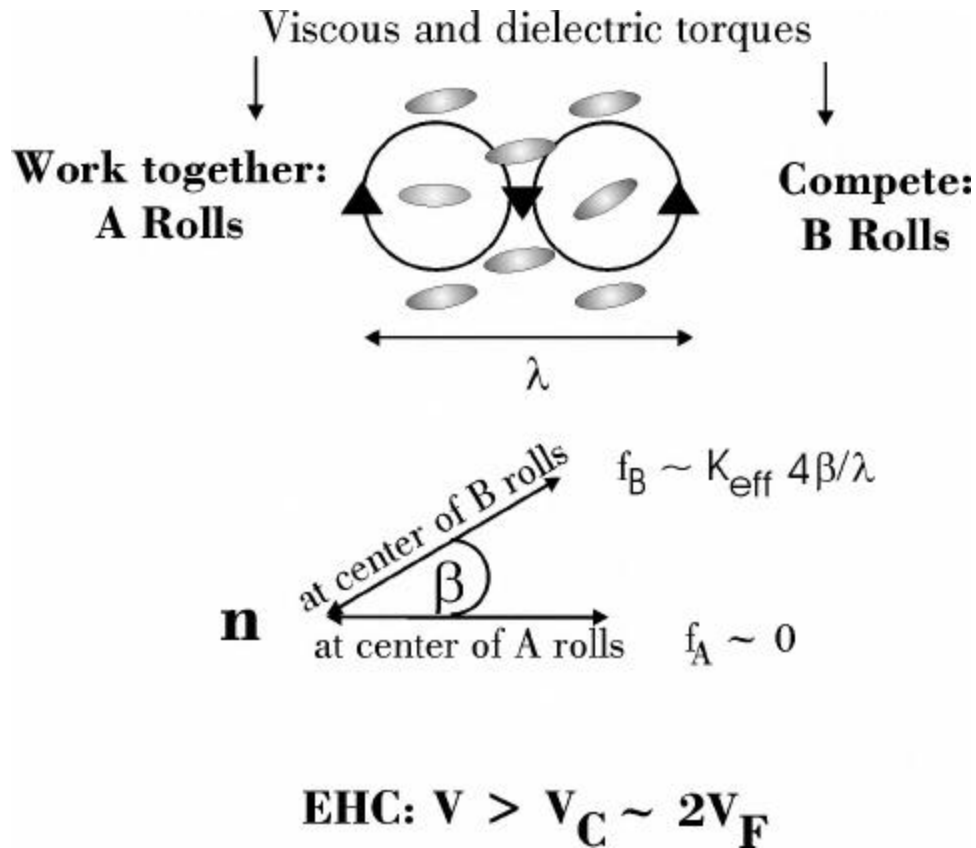
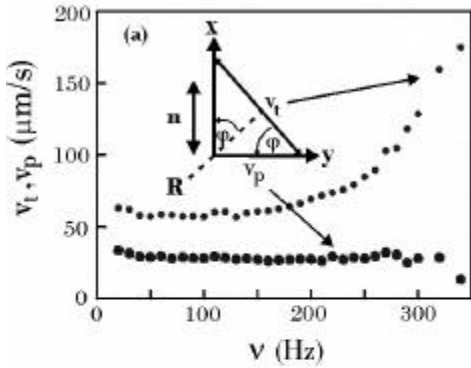


Fig. 5. For EHC patterns built on a nonlinear base state, we distinguish two kinds of rolls. In A rolls, viscous and dielectric torques work together while in B rolls, they compete. Assuming $n_x \approx 1$ everywhere except at the center of B rolls, we estimate the pattern speed from the energy density difference between A and B rolls: $f_B - f_A$.

The First Instability: Traveling Degenerate Rolls

The first instability built on the initially nonlinear base state (Fig. 4) [1] differs on several counts from that built on the initially uniform one (Fig. 3) [2]. First because of the boundary layer, its wavelength, λ , is nearly half that of λ_p for similar V and v . Second, \mathbf{R} is at an angle, $\pm \phi$ to \mathbf{n} (Figs. 1a, 4, 6). Third, the rolls travel with a velocity \mathbf{v}_t where $\mathbf{v}_t \perp \mathbf{R}$. As both $\pm v_t$ are observed, this is a Hopf bifurcation. Fourth, as \mathbf{R} becomes more normal to \mathbf{n} , the rolls travel faster (Fig. 6).

Pattern Travels



$$\begin{aligned}
 \mathbf{v}_p &\perp \mathbf{n} & v_p &= v_t \cos\phi \\
 \mathbf{v}_t &\perp \mathbf{R} \\
 K_{\text{eff}} &\sim \frac{K_3 + K_2}{2} \\
 v_p &\approx \frac{2}{d} \frac{K_{\text{eff}}}{\gamma_1} & \frac{v_t}{v_p} &\approx 2\beta \frac{d}{\lambda}
 \end{aligned}$$

$\beta \rightarrow \pi/2$
 Stationary
 Standing Stripe Pattern

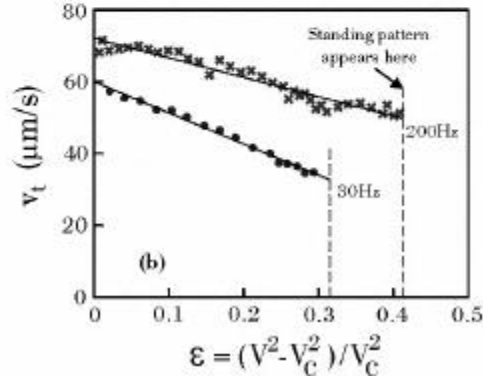


Fig. 6. $\mathbf{v}_t \perp \mathbf{R}$ and $\mathbf{v}_p \perp \mathbf{n}$ as a function of ν and \mathbf{v}_t vs. the control parameter, ϵ [1]. The estimate for v_t is based on the geometry shown in Fig. 5.

But the pattern velocity, $\mathbf{v}_p \perp \mathbf{n}$ ($v_p \equiv v_t \cos \phi = 32 \mu\text{m/s}$) is independent of ν (Fig. 6). The only length scale independent of ν in this problem is d . Also deformations $\perp \mathbf{n}$ involve all elastic constants: K_1 (splay), K_2 (twist) and K_3 (bend), giving the estimate for v_p shown in Fig. 6 [1].

We estimate v_t from the mismatch in curvature elasticity between the A and B rolls (Figs. 5, 6) to obtain $v_t / v_p \approx 2 \beta (d / \lambda)$ [1]. Consistent with observations, the smaller

Wavelength Doubling to Möbius Defect Turbulence

λ , the larger v_t . (Fig. 6). An order of magnitude estimate for v_t is found by putting $\beta \approx 1$. Then, $v_t \sim 60 \mu\text{m/s}$ at $\nu = 10 \text{ Hz}$ where $\lambda / d \approx 1.1$ and increases to $v_t \approx 90 \mu\text{m/s}$ at 300Hz where $\lambda / d \sim 0.7$. This estimate is surprisingly good at 10Hz and less so at 300Hz (Fig. 6). The implication is that a large enough β / λ ratio is needed to trigger the novel Standing Stripe Pattern which is not observed at any voltage when $\nu \leq 200 \text{ Hz}$ [5].

The Second Instability: The Standing Stripe Pattern

A subcritical bifurcation launches the second instability when $0.40 < \nu / \nu_c < 0.78$ and $25\text{V} < V \equiv V_s < 50\text{V}$ (Figs. 1b, 7). In the novel Standing Stripe Pattern (Fig. 7), \mathbf{n} has a small periodic component parallel to the roll axes ($n_y \neq 0$). This is a consequence of homeotropic boundary conditions which allow \mathbf{n} complete xy -freedom. Optical analysis shows maximum and minimum values of n_y associated with only one roll of a roll pair. We identify these particular rolls as the more energetic B rolls (Fig. 5) of the first pattern. The stripe pattern wavelength, λ_s , is thus, $\lambda_s = 2\lambda \sim 24 \mu\text{m} \gtrsim d$ (Fig. 7).

Standing Stripe Pattern

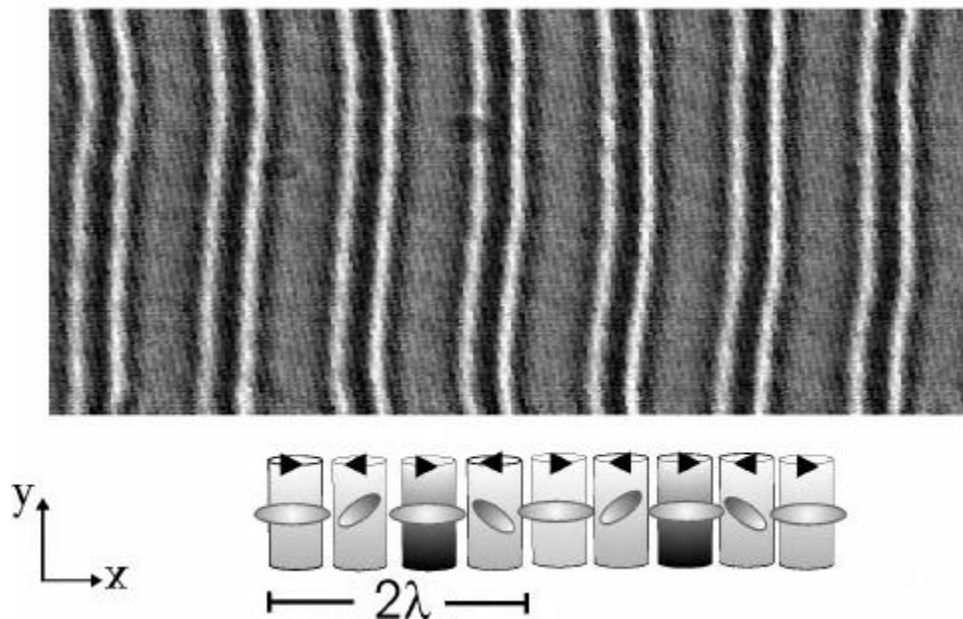


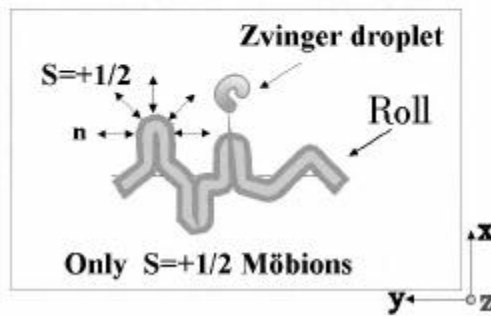
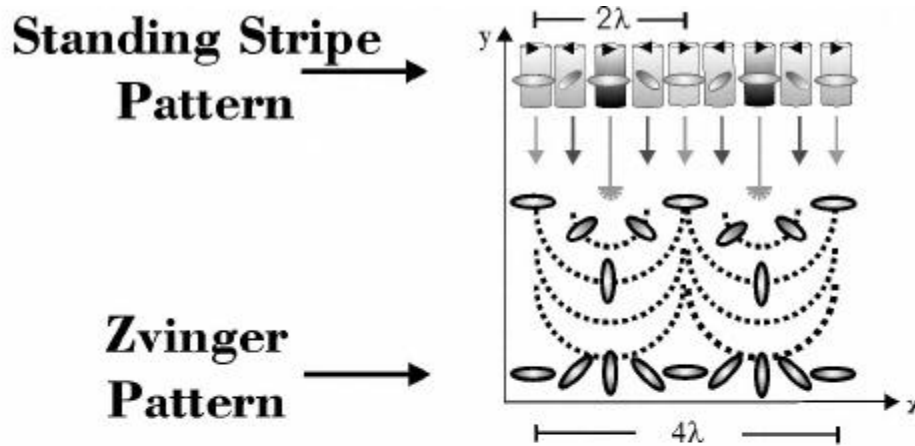
Fig. 7. The director orientation at the roll centers of the Standing Stripe Pattern shown bottom [1].

The Third Instability: The Zvinger Pattern

With only weak elastic forces stabilizing it, the Standing Stripe Pattern occurs in a narrow voltage range and subcritically bifurcates to the Zvinger Pattern (Fig. 1c) when $V = V_z \approx 1.1 V_s$. The Zvinger pattern forms when the B rolls (i.e. those rolls with maximum and minimum n_y) in the Standing Stripe Pattern rotate in opposite directions

to form roll arcs and Möbions, the $S = +\frac{1}{2}$ defects (Fig. 8). With one Möbion every λ_s , $\lambda_z = 2\lambda_s = 4\lambda \sim 40 \mu\text{m} \sim 2d$ (Figs. 1c and 8). While now in the plane of shear, $\mathbf{n} \perp \mathbf{R}$, \mathbf{n} rotates 2π in λ_z (Fig. 8).

The uniform rotation of \mathbf{n} in a Zvinger is beautifully revealed when the field is turned off (Fig. 2). Möbions associated with Zvinger dislocations are also seen. The repulsive interactions observed between Möbions is additional evidence that they all bear the same topological charge.



Möbions with the SAME Topological Charge

Fig. 8: Transition from the Standing Stripe Pattern to the Zvinger Pattern [1]. Roll disclinations formed by one roll all have the same topological charge, $S = +1/2$.

Fourth Instability: Transition to Möbius Defect Turbulence

Fig. 1d shows fully-developed Zvingers close to the transition to Möbius defect turbulence (Fig. 2). In Fig. 1d, the pattern wavelength is close to $2\lambda_z$ of the Zvinger pattern at onset.

CONCLUSIONS

Roll patterns built on a nonlinear base state dramatically contrast with those built on an initially uniform one. The first instability is a Hopf bifurcation. Further from equilibrium, the oscillatory pattern subcritically bifurcates to a novel Standing Stripe Pattern that in turn has a subcritical bifurcation to a curved roll pattern (Zvingers). These results provide complementary information for theories based on small amplitude perturbations of a highly nonlinear base state.

Acknowledgements: PEC thanks the Organizers of **ILCC98** for support.

REFERENCES

1. C. Fradin, P. L. Finn, H. R. Brand and P. E. Cladis, *Phys. Rev. Lett.* **81**, 2902 (1998).
2. H. R. Brand, C. Fradin, P. L. Finn, W. Pesch and P. E. Cladis, *Phys. Lett.* **A235**, 508 (1997).
3. P. G. de Gennes and J. Prost, *The Physics of Liquid Crystals* (Clarendon Press, Oxford 1993) 2nd Edition.
4. S. Kai and W. Zimmermann, *Prog. Theor. Phys. Suppl.* **99**, 458 (1989); L. Kramer and W. Pesch, *Ann. Rev. Fluid Mech.* **27**, 515 (1995).
5. C. Fradin et al. (*unpublished*).
6. P. Keller, P. E. Cladis, P. L. Finn and H. R. Brand, *J. Phys (Paris)* **46**, 2203 (1985).
7. 10E6: *4'-hexyloxyphenyl 4-decyloxybenzoate*. This compound was synthesized by E. Chin and J. W. Goodby.
8. A. Hertrich, W. Decker, W. Pesch and L. Kramer, *J. Phys. (France) II* **2**, 1915 (1992); A. Hertrich, *private communication*.
9. H. Richter, N. Kloepper, A. Hertrich and A. Buka, *Europhys. Lett.* **30**, 37 (1995).
10. S. Kai, K. Hayashi and Y. Hidaka, *J. Phys. Chem.* **100**, 19007 (1996).